DOI: https://doi.org/10.57233/ijsgs.v12i2.1113

ISSNp: 2488-9229; ISSNe: 3027-1118

IJSGS FUGUSAU VOL . 12 (2) WEBSITE: https://fugus-ijsgs.com.ng

INTERNATIONAL JOURNAL OF SCIENCE FOR GLOBAL SUSTAINABILITY

(A PUBLICATION OF FACULTY OF SCIENCE, FEDERAL UNIVERSITY GUSAU, NIGERIA)

# MHD Casson Fluid flow Past a Vertical Plate in the Presence of Heat Source/Sink, Viscous Dissipation and Mass Absorption

**[1]Omokhuale, Emmanuel and [2]Maduka, N. C.**

[1]Department of Mathematical Sciences, Federal University Gusau, P. M. B. 1001, Zamfara State, Nigeria.

[2]Department of Physics, Federal University Gusau, P. M. B. 1001, Zamfara State, Nigeria.

**Corresponding Author's Email**: emmanuelomokhuale@fugusau.edu.ng , emmanuelomokhuale@gmail.com

**Received on:** April 2026 **Revised and Accepted on:** June, 2026 **Published on:** July, 2026

***ABSTRACT***

A numerical investigation based on the finite difference method was conducted to examine the combined effects of mass absorption and viscous dissipation on unsteady magnetohydrodynamic (MHD) Casson fluid flow over a vertical plate embedded in a porous medium in the presence of a heat source/sink. The governing dimensionless, nonlinear, coupled partial differential equations describing the flow were solved numerically using the implicit Crank–Nicolson finite difference scheme. The influences of the governing flow parameters on the velocity, temperature, and concentration distributions were analyzed and presented graphically. The numerical results indicate that increasing the Casson parameter, mass absorption parameter, viscous dissipation parameter, and heat source parameter enhances both the velocity and temperature distributions. In contrast, an increase in the heat sink parameter suppresses fluid motion by reducing the velocity profile. Furthermore, higher values of the chemical reaction parameter and Schmidt number significantly diminish both the concentration and velocity distributions due to reduced species diffusion and weakened concentration-induced buoyancy effects. The findings of this study have potential applications in several engineering and biomedical fields, including glass manufacturing, petroleum refining, lubrication systems, paper production, and the analysis of blood flow in cardiovascular devices.

**Keywords:** MHD; Casson fluid; Viscous dissipation; Finite difference method; Heat source/sink.

## 1.0 INTRODUCTION

Magnetohydrodynamic (MHD) Casson fluid flow over a vertical plate in the presence of heat source/sink, viscous dissipation, and mass absorption represents a complex transport phenomenon with important applications in engineering and biomedical sciences. This model describes the flow behavior of electrically conducting non-Newtonian fluids, such as blood, polymer melts, drilling muds, and other industrial suspensions, under the combined influence of magnetic fields and thermal effects. Advances in modern technology have intensified research interest in MHD flows of non-Newtonian fluids owing to their broad range of practical applications. Compared with Newtonian fluids, highly viscous non-Newtonian fluids exhibit more complex rheological characteristics, making them particularly suitable for applications in physiological processes, pharmaceutical manufacturing, biomedical engineering, food processing, materials processing, and other industrial operations (Reddy *et al.*, 2025). Non-Newtonian fluids are classified into several categories, including couple stress, micropolar, power-law, Reiner–Philippoff, Williamson, Sisko, Oldroyd-B, Jeffrey, Maxwell, and Casson fluids, each possessing unique rheological properties. Among these models, the Casson fluid has received considerable attention because of its ability to accurately characterize yield stress behavior. Originally proposed by Casson in 1957, the model describes fluids that behave as rigid bodies until the applied shear stress exceeds a critical yield stress, after which they begin to flow. Materials exhibiting Casson fluid characteristics include blood, honey, jelly, polymer solutions, printer inks, gypsum paste, cosmetic creams, and certain ceramic suspensions (Reddy *et al.*, 2025). Owing to its practical significance, the Casson fluid model has been widely employed to investigate complex transport phenomena involving magnetic fields, heat transfer, and mass transfer. For instance, Reddy and Goud (2026) numerically examined the transport characteristics of MHD Casson fluid flow over an exponentially stretching surface, considering the combined effects of viscous dissipation, thermal radiation, Dufour diffusion, and activation energy. Their findings further demonstrated the importance of incorporating multiple physical mechanisms when modeling non-Newtonian fluid flows encountered in advanced engineering and industrial processes.

Viscous dissipation plays a significant role in modifying the thermal characteristics of a fluid by converting mechanical energy into internal thermal energy, thereby enhancing the heat transfer process. This phenomenon has important applications in numerous engineering systems, including electronic cooling devices, paper manufacturing, material processing, lubrication, tribology, and thermal management technologies. Furthermore, the combined effects of viscous dissipation

DOI: https://doi.org/10.57233/ijsgs.v12i2.1113 ISSNp: 2488-9229; ISSNe: 3027-1118
IJSGS FUGUSAU VOL . 12 (2) WEBSITE: https://fugus-ijsgs.com.ng

and thermal radiation are of considerable importance in scientific, industrial, and engineering processes involving high temperatures, such as metal casting, furnace design, instrumentation, polymer processing, missile technology, and solar energy systems. Although several studies have investigated heat and mass transfer in Casson fluid flows, the influence of viscous dissipation has not been comprehensively examined in many existing models. Given its significant impact on thermal transport and fluid behavior, incorporating viscous dissipation into heat and mass transfer analyses provides a more realistic representation of practical flow systems (Reddy *et al.*, 2024). In this context, Mohammed *et al.* (2026) investigated the flow of Casson fluid over a stretching sheet by examining the effects of the Casson parameter, magnetic field, porous medium, and viscous dissipation on the flow characteristics. Similarly, Reddy *et al.* (2024) numerically analyzed the combined effects of heat generation, buoyancy forces, viscous dissipation, and Joule heating on unsteady hydromagnetic mixed convection of a chemically reactive and radiative Casson fluid flowing over an exponentially accelerating permeable vertical plate embedded in a porous medium, while considering ramped surface temperature and concentration conditions. The governing dimensionless nonlinear coupled partial differential equations were solved using the implicit Crank–Nicolson finite difference method. More recently, Kumar and Shekar (2026) examined the effects of chemical reaction, thermal radiation, and mass transfer on unsteady magnetohydrodynamic (MHD) Casson fluid flow past a vertical porous plate in the presence of heat generation and viscous dissipation. In their formulation, the fluid was assumed to be incompressible and electrically conducting, while thermal radiation was modeled using the Rosseland diffusion approximation. These studies collectively demonstrate the importance of incorporating viscous dissipation and related transport mechanisms when modeling heat and mass transfer in electrically conducting non-Newtonian fluids.

Heat source and heat sink mechanisms play a significant role in regulating the thermal characteristics of fluid flow. A heat source supplies thermal energy to the fluid, thereby increasing its temperature and enhancing the thermal boundary layer, whereas a heat sink extracts thermal energy, leading to a reduction in fluid temperature and a thinner thermal boundary layer. Investigating these thermal effects in magnetohydrodynamic (MHD) Casson fluid flow over exponentially stretching surfaces provides valuable insights into the design and optimization of thermal management systems for various engineering and industrial applications (Vinod *et al.*, 2025). Omokhuale and Jabaka (2022) studied unsteady convective Couette flow with heat sink and radiation effects numerically. Omokhuale and Dange (2025) examined effects of heat generation and Soret on MHD Couette flow with radiation and mass absorption In a related study, Reddy *et al.* (2025) investigated the combined effects of cross-diffusion, viscous dissipation, and an inclined magnetic field on Casson fluid flow over an oscillatory semi-infinite vertical surface under heat-loss conditions. The novelty of their work lies in the simultaneous incorporation of viscous heating, Soret and Dufour cross-diffusion effects, and magnetohydrodynamic interactions within a Casson fluid model, an area that has received relatively limited attention in the existing literature. Similarly, Vinod *et al.* (2025) analyzed the magnetohydrodynamic boundary-layer flow and heat transfer characteristics of a Casson fluid over an exponentially stretching sheet while accounting for thermal radiation and heat source/sink effects. Their findings demonstrated that these thermal mechanisms significantly influence the fluid flow and heat transfer behavior. More recently, Konda *et al.* (2025) conducted a numerical investigation of transverse MHD Casson fluid flow over a nonlinear expanding surface by considering the combined effects of thermal radiation, heat generation/absorption, and chemical reaction. Their study highlighted the importance of incorporating multiple interacting physical mechanisms to achieve a more accurate prediction of the thermal and hydrodynamic behavior of electrically conducting non-Newtonian fluids under complex flow conditions.

The finite difference method (FDM) is a well-established numerical technique for solving coupled nonlinear partial differential equations that are difficult or impossible to solve analytically. Owing to its accuracy, stability, and computational efficiency, FDM has been extensively employed in the numerical analysis of complex fluid flow and heat and mass transfer problems. For example, Omokhuale and Jabaka (2019) numerically investigated magnetohydrodynamic (MHD) Casson fluid flow over an infinite vertical plate in the presence of chemical reaction and heat generation using the finite difference method. In subsequent studies, the authors extended their model to incorporate additional physical effects, including thermal radiation, variable thermal conductivity, and chemical absorption (Omokhuale & Jabaka, 2020a, 2020b). A review of the existing literature reveals that most investigations on Casson fluid flow have primarily relied on analytical or semi-analytical solution techniques, while relatively few studies have employed numerical methods capable of addressing more complex flow configurations and coupled transport phenomena. This

DOI: https://doi.org/10.57233/ijsgs.v12i2.1113 ISSNp: 2488-9229; ISSNe: 3027-1118
IJSGS FUGUSAU VOL . 12 (2) WEBSITE: https://fugus-ijsgs.com.ng

limited application of numerical approaches highlights an important research gap in the literature.

Motivated by these observations, the present study extends the work of Omokhuale and Jabaka (2020a) by numerically investigating unsteady magnetohydrodynamic (MHD) Casson fluid flow past a vertical plate embedded in a porous medium, incorporating the effects of viscous dissipation, suction/injection, and heat source/sink. The governing equations are solved using the finite difference method to provide a comprehensive understanding of the coupled momentum, heat, and mass transfer processes. The inclusion of these additional physical mechanisms enhances the applicability of the model to practical engineering and industrial systems involving electrically conducting non-Newtonian fluids.

## 2.0 MATHEMATICAL FORMULATION

We consider Casson fluid over an infinite vertical plate embedded in a saturated porous medium. The flow being restricted to $y>0$, where $y$ is the coordinate which would be measured in the normal direction to the plate. The fluid is assumed to be electrically conducting with a uniform magnetic field $B$ of strength $B_0$, applied in a direction perpendicular to the plate. The plate temperature is raised to $T_w$ which is thereafter maintained constant.

The rheological equation of state for the Cauchy stress tensor of Casson fluid is given by,

$$\tau=\tau_0+\mu\tau^*$$

$$\text{where } \tau_0=\begin{cases} 2\left(\mu_B+\dfrac{p_y}{\sqrt{2\pi}}\right)e_{ij},\ when\ \pi>\pi_c \\ 2\left(\mu_B+\dfrac{p_y}{\sqrt{2\pi_c}}\right)e_{ij},\ when\ \pi<\pi_c \end{cases}$$

where $\pi=e_{ij}e_{ij}$ and $e_{ij}$ is the $(i,j)^{th}$ component of the deformation rate.

The following assumptions were made before deriving the governing equations; incompressible flow, free convection and non-Newtonian flow, infinite vertical plate, fluid suction/injection and magnetic field are imposed at the plate surface, the temperature and concentration of the fluid are raised to $T'_w$ and $C'_w$ respectively and are higher than the ambient temperature and that of fluid. In addition, the effects of chemical reaction, radiation are considered. It is also assumed that the viscous dissipation and heat surce/sink is present.

The governing equations of the flow under the usual Boussinesq and boundary-layer approximation can be written as:

$$\frac{\partial v'}{\partial y'}=0 \tag{1}$$

$$\rho\left(\frac{\partial u'}{\partial t'}+v'\frac{\partial u'}{\partial y'}\right)=\mu_B\left(1+\frac{1}{\alpha}\right)\frac{\partial^2 u'}{\partial y'^2}-\sigma B_0^2u'-\frac{\mu\eta}{K_1}\left(1+\frac{1}{\alpha}\right)u'$$
$$+g\rho\left[\beta_T\left(T'-T'_\infty\right)+\beta_m\left(C'-C'_\infty\right)\right] \tag{2}$$

$$\left(\frac{\partial T'}{\partial t'}+v'\frac{\partial T'}{\partial y'}\right)=\frac{k}{\rho Cp}\frac{\partial^2 T'}{\partial y'^2}-\frac{1}{\rho Cp}\frac{\partial q_r}{\partial y^*}+\frac{Q_T}{\rho Cp}\left(T'-T'_\infty\right)+\frac{Q_C}{\rho Cp}\left(T'-T'_\infty\right)+\frac{\mu}{Cp}\left(1+\frac{1}{\alpha}\right)\left(\frac{\partial u'}{\partial y'}\right)^2$$
$$+\frac{\mu}{Cp}\left(1+\frac{1}{\alpha}\right)\left(\frac{\partial u'}{\partial y'}\right)^2 \tag{3}$$

$$\frac{\partial C'}{\partial t'}+v'\frac{\partial C'}{\partial y'}=D\frac{\partial^2 C'}{\partial y'^2}-R^*\left(C'-C'_\infty\right) \tag{4}$$

with the following initial and boundary conditions:

$$\left.\begin{array}{l} t'\le 0, u'=0, T'\to T'_\infty, C'\to C'_\infty\ for\, all\ y' \\ t'>0, u'=u_p, T'=T'_w, C'=C'_w\ at\ y'=0 \\ \quad u'\to 0, T'\to T'_\infty, C'\to C'_\infty\ as\ y'\to\infty \end{array}\right\} \tag{5}$$

DOI: https://doi.org/10.57233/ijsgs.v12i2.1113 ISSNp: 2488-9229; ISSNe: 3027-1118
IJSGS FUGUSAU VOL . 12 (2) WEBSITE: https://fugus-ijsgs.com.ng

$v_0 > 0$ is the suction parameter and $v_0 < 0$ is the injection parameter.

For the case of an optically thin gray gas the local radiant absorption is expressed by

$$\frac{\partial q_r}{\partial y'} = -4a_R\sigma\left(T_\infty'^4 - T'^4\right) \tag{6}$$

we assume that the temperature difference within the flow are sufficiently small such that $T'^4$ may be expressed as a linear function of the temperature. This is accomplished by expanding $T'^4$ in Taylor series about $T'_\infty$ and neglecting higher-order terms, thus

$$T'^4 \cong 4T_\infty'^3 T' - 3T_\infty'^4 \tag{7}$$

By using equations (6) and (7), equation (2) reduces to

$$\left[\frac{\partial T'}{\partial t'} + v\frac{\partial T'}{\partial y'}\right] = \frac{k_o}{\rho Cp}\frac{\partial^2 T'}{\partial y'^2} - \frac{16a_R\sigma T_\infty'^3}{\rho Cp}\left(T' - T'_\infty\right) + \frac{Q}{\rho Cp}\left(T' - T'_\infty\right) + \nu\left(\frac{\partial u'}{\partial y'}\right)^2 \tag{8}$$

On introducing the following non-dimensionless quantities

$$\left.\lambda = \frac{u_0}{\nu}y', u_p = \frac{u_p'}{u_0}, t = \frac{u_0^2}{\nu}t', \varphi = \frac{u'}{u_0}, \phi = \frac{T' - T'_\infty}{T_w - T_\infty}, \chi = \frac{C' - C'_\infty}{C_w - C_\infty}, \tau^* = \frac{\tau}{\rho u^2}\right\} \tag{9}$$

Using (1) and (9), equations (3) - (5) and (8) is transformed to:

$$\frac{\partial \varphi}{\partial t} \pm \lambda\frac{\partial \varphi}{\partial \lambda} = \left(1 + \frac{1}{\alpha}\right)\frac{\partial^2 \varphi}{\partial \lambda^2} - \left[M + \left(1 + \frac{1}{\alpha}\right)\frac{1}{K_M}\right]\varphi + G_T\phi + G_m\chi \tag{10}$$

$$\frac{\partial \phi}{\partial t} \pm \lambda\frac{\partial \phi}{\partial \lambda} = \frac{1}{\Pr}\frac{\partial^2 \phi}{\partial \lambda^2} - \frac{R}{\Pr}\phi \pm \gamma_1\phi + \gamma_2\chi + Ec\left(1 + \frac{1}{\alpha}\right)\left(\frac{\partial \varphi}{\partial \lambda}\right)^2 \tag{11}$$

$$\frac{\partial \chi}{\partial t} \pm \lambda\frac{\partial \chi}{\partial \lambda} = \frac{1}{Sc}\frac{\partial^2 \chi}{\partial \lambda^2} - \xi\chi \tag{12}$$

The corresponding boundary conditions are:

$$\left.\begin{array}{l} \varphi = 0, \phi = 0, \chi = 0 \; for\; all\; \lambda, t \le 0 \\ \varphi = 0, \phi = 1, \chi = 1 \; at\; \lambda = 0 \\ \varphi \to 0, \phi \to 0, \chi \to 0 \; as\; \lambda \to \infty \end{array}\right\} \tag{13}$$

where $\alpha$ is the Casson parameter, $G_T$ is the thermal Grashof number, $G_m$ is the mass Grashof number, $Sc$ is the Schmidt number, $\Pr$ is the Prandtl number, $M$ is the magnetic parameter, $\xi$ is the chemical reaction parameter, $K$ is the permeability parameter, $\lambda$ is the suction parameter, $\gamma_1$ is the heat generation/absorption parameter, $\gamma_2$ is the mass absorption parameter, $Ec$ is the Eckert number parameter and $\gamma_2$ is the mass absorption parameter.

## 3.0 COMPUTATIONAL TECHNIQUE

To get the difference equations, the region of the flow is divided into a grid or mesh of line parallel to $\lambda$ axis. Where $\lambda$-axis is normal to the plate. It is considered that the plate is of height $\lambda_{\max} = 150$ i.e. $\lambda$ varies from 1 to 150. There are $m = 150$ and $n = 300$ grid spacing in the $\lambda$-directions. It is assumed that $\Delta\lambda$ is a constant mesh size along $\lambda$ direction and taken as $\lambda = 0.50(0 \le \lambda \le 150)$. with the smaller time-step, $\Delta t = 0.0005$ and $u', T'$ and $C'$ represents the values of $\varphi, \phi$ and $\chi$ at the end of a time step, respectively.

Therefore, the nonlinear coupled partial differential equations (10) to (12) subject to boundary conditions (13) are solved numerically using explicit finite difference method as below:

DOI: https://doi.org/10.57233/ijsgs.v12i2.1113 ISSNp: 2488-9229; ISSNe: 3027-1118
IJSGS FUGUSAU VOL . 12 (2) WEBSITE: https://fugus-ijsgs.com.ng

$$\left(\frac{\varphi_j^{i+1}-\varphi_j^i}{\Delta t}\pm\lambda\frac{\varphi_{j+1}^i-\varphi_j^i}{\Delta\lambda}\right)=\left(1+\frac{1}{\alpha}\right)\left[\frac{\varphi_{j-1}^i-2\varphi_j^i+\varphi_{j+1}^i+\varphi_{j-1}^{i+1}-2\varphi_j^{i+1}+\varphi_{j+1}^{i+i}}{(2\Delta\lambda)^2}\right]$$
$$-\left[M+\left(1+\frac{1}{\alpha}\right)\left(\frac{1}{K_M}\right)\right]\left(\frac{\varphi_j^i+\varphi_j^{i+1}}{2}\right)+G_T\left(\frac{\phi_j^i+\phi_j^{i+1}}{2}\right)+G_m\left(\frac{\chi_j^i+\chi_j^{i+1}}{2}\right)\quad(14)$$

$$\left(\frac{\phi_j^{i+1}-\phi_j^i}{\Delta t}\pm\lambda\frac{\phi_{j+1}^i-\phi_j^i}{\Delta\lambda}\right)=\frac{1}{\Pr}\cdot\left[\frac{\phi_{j-1}^i-2\phi_j^i+\phi_{j+1}^i+\phi_{j-1}^{i+1}-2\phi_j^{i+1}+\phi_{j+1}^{i+i}}{(2\Delta\lambda)^2}\right]-\frac{R}{\Pr}\left(\frac{\phi_j^i+\phi_j^{i+1}}{2}\right)+\gamma_1\left(\frac{\phi_j^i+\phi_j^{i+1}}{2}\right)+\gamma_2\left(\frac{\chi_j^i+\chi_j^{i+1}}{2}\right)$$
$$+Ec\left(1+\frac{1}{\alpha}\right)\left(\frac{\phi_{j+1}^i-\phi_j^i}{\Delta\lambda}\right)^2\quad(15)$$

$$Sc\left(\frac{\chi_j^{i+1}-\chi_j^i}{\Delta t}\pm\lambda\frac{\chi_{j+1}^i-\chi_j^i}{\Delta\lambda}\right)=\left[\frac{\chi_{j-1}^i-2\chi_j^i+\chi_{j+1}^i+\chi_{j-1}^{i+1}-2\chi_j^{i+1}+\chi_{j+1}^{i+i}}{(2\Delta\lambda)^2}\right]-\xi Sc\left(\frac{\chi_j^i+\chi_j^{i+1}}{2}\right)\quad(16)$$

The initial and boundary conditions becomes

$$\varphi_{i,0}=0,\phi_{i,0}=0,\chi_{i,0}=0 \text{ for all i except } i=0$$
$$\varphi_{i,0}=0,\phi_{i,0}=1,\chi_{i,0}=1\quad(17)$$
$$\varphi_{F,0}=0,\phi_{F,0}=1,\chi_{F,0}=1$$

where F corresponds to $\infty$. The suffix i corresponds to $\lambda$ and j is equals to t. consequently, $\Delta t=t_{j+1}-t_j$ and $\Delta\lambda=\lambda_{i+1}-\lambda_i$.

The finite difference approximations of these equations were solved by using the values for $G_T=1, G_m=1, \pm\gamma_1=1, \gamma_2=1, E_c=0.5, \alpha=1, \eta=1, Pr=0.71, Sc=0.66$, except where they are varied. A step size of $\Delta\lambda=0.01$ is used for the interval $\lambda_{\min}=0$ to $\lambda_{\max}=7$ for a desired accuracy and a convergence criterion of $10^{-6}$ is satisfied for various parameters.

## 4.0 DISCUSSION OF FINDINGS

To elucidate the physical characteristics of the proposed model, a comprehensive parametric study was conducted to examine the effects of several governing parameters on the flow behavior. These parameters include the Casson parameter, thermal and mass Grashof numbers, permeability (porosity) parameter, magnetic parameter, Eckert number, heat generation and heat absorption parameters, mass absorption parameter, chemical reaction parameter, as well as the Prandtl and Schmidt numbers. Their influences on the velocity, temperature, and concentration distributions of the Casson fluid were systematically investigated. Numerical solutions for the governing flow variables were computed, and the resulting profiles were presented through graphical illustrations and tabulated data to facilitate interpretation. The numerical simulations were performed by assigning the following baseline values to the governing dimensionless parameters like: $G_T=1, G_m=1, \pm\gamma_1=1, \gamma_2=1, E_c=0.5, \alpha=1, \eta=1, Pr=0.71, Sc=0.66$. The interval $Y_{\min}=0$ to $Y_{\max}=7$ for a desired accuracy and a convergence for various parameters.

Figures 1 to 14 are sketched to analyze the influent of $G_T, G_m, \pm\gamma_1, \gamma_2, E_c, \alpha, \eta, Pr, Sc$ on Casson fluid velocity $\varphi$, temperature $\phi$ and concentration $\chi$ against $\lambda$.

Figures 1 and 2 present the velocity profiles corresponding to different values of the thermal Grashof number $(G_T)$and mass Grashof number $(G_m)$, respectively. The results indicate that the fluid velocity increases with increasing values of both parameters. This trend is attributed to the enhancement of thermal and concentration-induced buoyancy forces, which promote fluid acceleration by overcoming viscous resistance, thereby increasing the velocity throughout the boundary layer. Figures 3 and 4 illustrate the effects of the heat generation and heat absorption parameters on the fluid velocity distribution, respectively. It is observed that increasing the heat generation parameter significantly reduces the fluid velocity. Conversely, an increase in the heat absorption parameter enhances the fluid velocity,

DOI: https://doi.org/10.57233/ijsgs.v12i2.1113 ISSNp: 2488-9229; ISSNe: 3027-1118

IJSGS FUGUSAU VOL . 12 (2) WEBSITE: https://fugus-ijsgs.com.ng

producing an opposite trend in the flow field. Figure 5 shows the effect of the chemical absorption parameter on the velocity profile. The results demonstrate that increasing the chemical absorption parameter leads to an enhancement in the fluid velocity. This behavior indicates that chemical absorption alters the flow characteristics by promoting momentum transport, thereby increasing the velocity throughout the boundary layer. Figures 6 and 7 depict the effects of the viscous dissipation parameter $(Ec)$and the Casson parameter $(\beta)$on the velocity distribution, respectively. The results indicate that the fluid velocity increases with increasing values of both $Ec$and $\beta$. The enhancement in velocity with increasing Eckert number is attributed to the conversion of kinetic energy into thermal energy through viscous dissipation, which intensifies the buoyancy forces and accelerates the fluid motion. Similarly, higher values of the Casson parameter improve the velocity profile by modifying the rheological characteristics of the fluid. As the Casson parameter increases, the yield stress and effective plastic dynamic viscosity are altered, facilitating greater momentum transport and consequently enhancing the fluid velocity throughout the boundary layer.

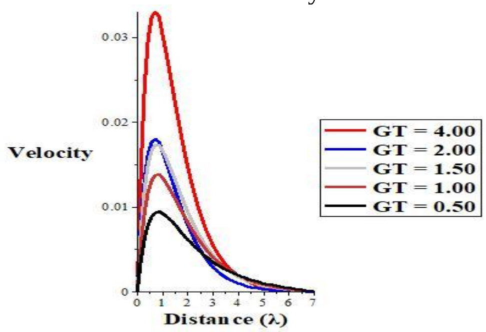


Figure 1: Velocity vs $\lambda$ for varying $G_T$

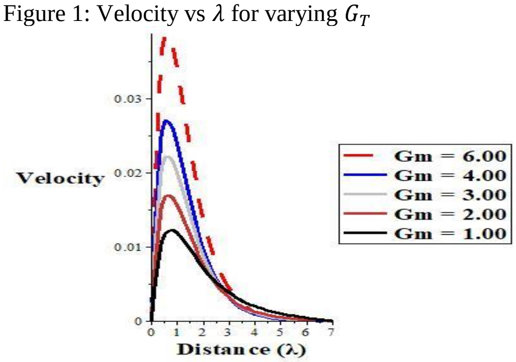


Figure 2: Velocity vs $\lambda$ for varying $G_m$

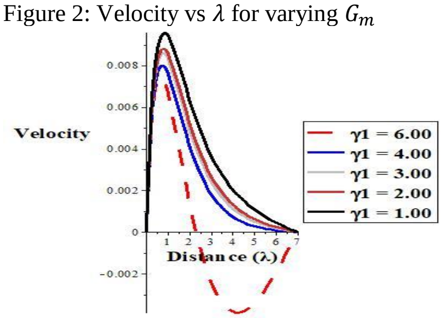


Figure 3: Velocity vs $\lambda$ for varying $\gamma_1 > 0$

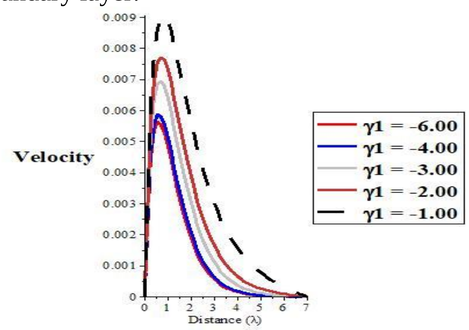


Figure 4: Velocity vs $\lambda$ for varying $\gamma_1 < 0$

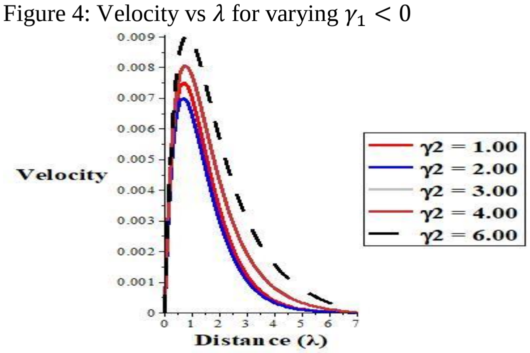


Figure 5: Velocity vs $\lambda$ for varying $\gamma_2$

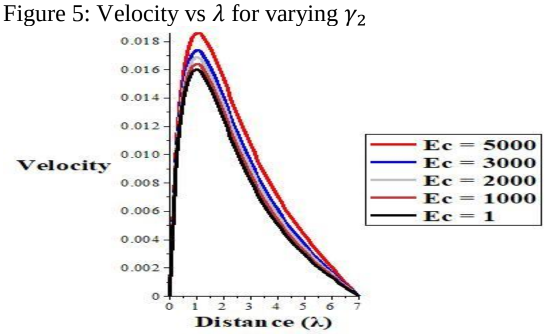


Figure 6: Velocity vs $\lambda$ for varying $E_c$

DOI: https://doi.org/10.57233/ijsgs.v12i2.1113 ISSNp: 2488-9229; ISSNe: 3027-1118
IJSGS FUGUSAU VOL . 12 (2) WEBSITE: https://fugus-ijsgs.com.ng

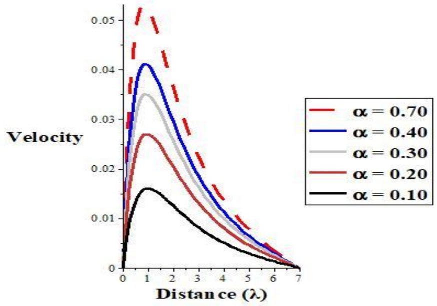


Figure 7: Velocity vs $\lambda$ for varying $\alpha$

Figure 8 demonstrates the influence of the Prandtl number $(Pr)$on the temperature distribution. It is observed that the fluid temperature decreases with increasing values of the Prandtl number. This behavior is attributed to the reduction in thermal diffusivity associated with higher Prandtl numbers, which suppresses heat diffusion and consequently reduces the thermal boundary layer thickness.

Figures 9 and 10 gives the effects of the heat generation and heat absorption parameters on the temperature distribution, respectively. The results indicate that increasing the heat generation parameter significantly reduces the fluid temperature. In contrast, increasing the heat absorption parameter produces the opposite effect by enhancing the temperature profile throughout the boundary layer. These contrasting trends demonstrate the significant influence of internal heat generation and heat absorption on the thermal characteristics of the flow. Figures 11 and 12 elucidate the effects of the chemical absorption parameter $(\gamma_2)$and the Eckert number $(Ec)$on the temperature distribution, respectively. The results reveal that the fluid temperature increases with increasing values of both $\gamma_2$and $Ec$. This behavior can be attributed to the enhanced thermal energy generated by chemical absorption and viscous dissipation. As the chemical absorption parameter increases, the energy released within the fluid raises the thermal energy of the fluid particles, leading to higher temperature profiles. Similarly, an increase in the Eckert number signifies greater conversion of kinetic energy into internal energy through viscous dissipation, thereby elevating the fluid temperature. The resulting increase in thermal energy intensifies the buoyancy forces, which consequently promotes fluid motion and enhances the velocity field.

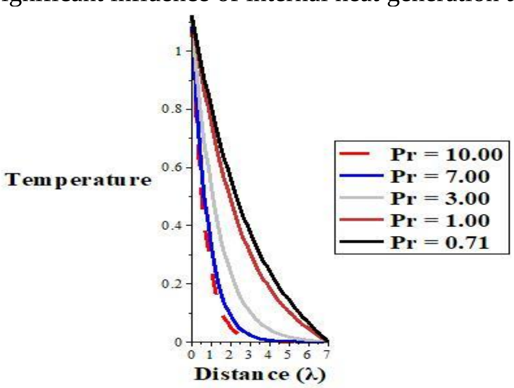


Figure 8: Temperature vs $\lambda$ for varying $P_r$

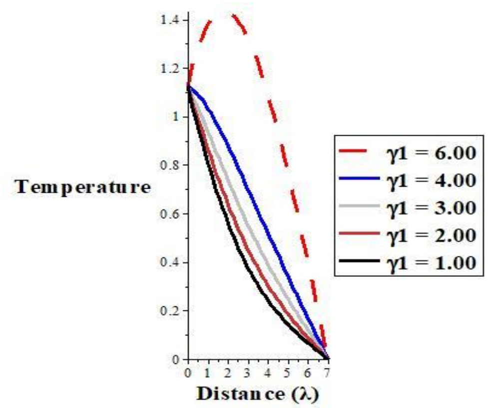


Figure 9: Temperature vs $\lambda$ for varying $\gamma_1 > 0$

DOI: https://doi.org/10.57233/ijsgs.v12i2.1113 ISSNp: 2488-9229; ISSNe: 3027-1118

IJSGS FUGUSAU VOL . 12 (2) WEBSITE: https://fugus-ijsgs.com.ng

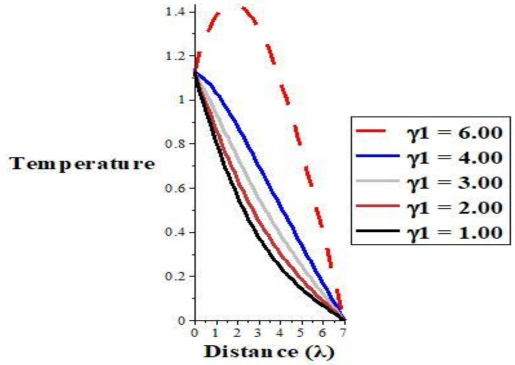


Figure 10: Temperature vs $\lambda$ for varying $\gamma_1 < 0$

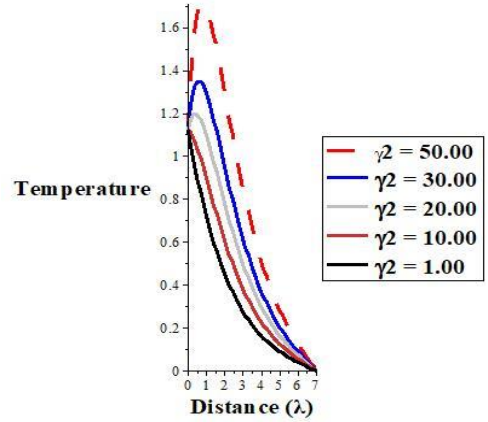


Figure 11: Temperature vs $\lambda$ for varying $\gamma_2$

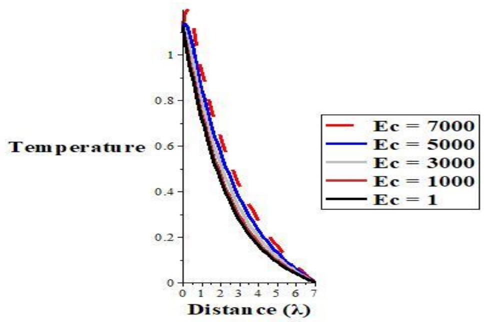


Figure 12: Temperature vs $\lambda$ for varying $E_c$

Figures 13 and 14 connotes the effects of the Schmidt number $(Sc)$and the chemical reaction parameter $(\eta)$on the concentration distribution, respectively. The results indicate that the concentration profile decreases with increasing values of both $Sc$and $\eta$. This behavior is physically expected because a higher Schmidt number corresponds to lower mass diffusivity, thereby reducing the rate of species diffusion within the fluid. Likewise, an increase in the chemical reaction parameter accelerates the consumption of the diffusing species, leading to a further reduction in concentration. Consequently, the concentration boundary layer becomes thinner, resulting in weaker concentration-induced buoyancy effects and a corresponding reduction in fluid motion.

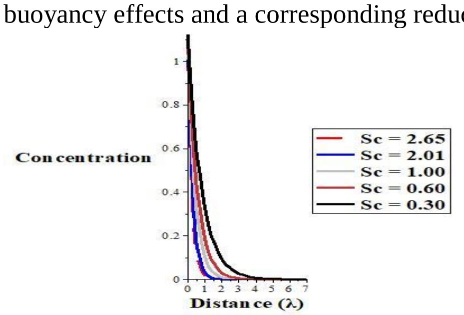


Figure 13: Concentration vs $\lambda$ for varying $S_C$

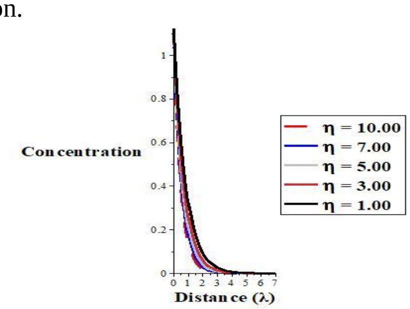


Figure 14: Concentration vs $\lambda$ for varying $\eta$

## 5.0 CONCLUDING REMARKS

In this study, the governing nonlinear partial differential equations describing the magnetohydrodynamic (MHD) flow of a Casson fluid with viscous dissipation, mass absorption, and heat source/sink effects were solved numerically. Understanding the transport characteristics of reactive-radiative MHD Casson fluid flows is of considerable importance in numerous engineering and industrial applications, including space technology, lubrication systems, tribology, pharmaceutical and biomedical processes, as well as high-temperature operations such as glass manufacturing, furnace engineering, and fire dynamics. Based on the numerical analysis, the following major findings are drawn:

(i) The fluid velocity increases with increasing values of the thermal Grashof number $(G_T)$, mass Grashof number $(G_m)$, heat absorption parameter $(+\gamma_1)$, chemical absorption parameter $(\gamma_2)$, Eckert number $(E_c)$, and Casson parameter $(\alpha)$. In contrast, increasing the heat generation parameter $(-\gamma_1)$suppresses the fluid velocity.

(ii) The temperature distribution is enhanced by increasing the heat absorption parameter $(+\gamma_1)$, chemical absorption parameter $(\gamma_2)$, and Eckert number $(E_c)$. Conversely, higher values of the heat generation parameter $(-\gamma_1)$and the Prandtl number $(Pr)$reduce the temperature distribution and consequently decrease the thermal boundary-layer thickness.

(iii) Increasing the Schmidt number $(Sc)$and the chemical reaction parameter significantly reduces the concentration profile, resulting in a thinner concentration boundary layer due to the suppression of species diffusion.

## 6.0 FUTURE SUGGESTIONS

The present study may be extended in several directions to broaden its applicability and enhance its contribution to the field of fluid mechanics. Specifically:

(i) Future investigations may consider other non-Newtonian fluid models, such as the Walter's-B, second-grade, Jeffrey, Maxwell, and Oldroyd-B fluids, to examine the influence of different rheological characteristics on heat and mass transfer phenomena.

(ii) The governing equations may be further enriched by incorporating cross-diffusion effects, namely the Soret (thermo-diffusion) and Dufour (diffusion-thermo) effects, to provide a more comprehensive description of coupled heat and mass transfer processes.

(iii) The current model may also be extended to investigate various nanofluid and hybrid nanofluid models, enabling the assessment of their heat and mass transfer characteristics in diverse engineering, biomedical, and industrial applications.

## 6.0 ACKNOWLEDGEMENTS

The authors are grateful to Tertiary Education Trust Fund (TETFUND) and the management of Federal University Gusau, Nigeria. for funding this research work under the Institutional Based Research **(TETF/DR&D/CE/UNI/GUSAU/IBR/2026/VOL.1)**.

## REFERENCES

Kumar, V. V., & Shekar, M. R. (2026). Effects of chemical reactions, radiative heat transfer, and mass transfer on unsteady MHD Casson fluid flow past a porous plate with heat generation and dissipation. Advanced Engineering Sciences, 58(1), 1249-1261.

Konda, J., Ganteda, C., Salleh, Z., Sundaram, I., Inc, M., Ramakrishna, B., ... & Govindan, V. (2025). Impact of radiation and heat source/sink on dissipative MHD mixed convection flow of casson nanofluid over a stretching sheet with chemical reaction. Journal of Radiation Research and Applied Sciences, 18(3).https://doi.org/10.1016/j.jrras.2025.101584

Mohammed, I., Manko, A., & Jibrin, K. (2026). MHD Casson Fluid Flow Over A Linear Stretching Sheet With The Effect Of Viscous Dissipation. International Journal of Nature and Science Advance Research, 12(9). https://doi.org /10.70382/meinsar.v12i9.082

Omokhuale, E., & Jabaka, M. L. (2019). Magnetohydrodynamic Casson Fluid Flow over an Infinite Vertical Plate with Chemical Reaction and Heat Generation. American Journal of Computational Mathematics, 9(3), 187-200. https://doi.org/10.4236/ajcm.2019.93014

Omokhuale, E., & Jabaka, M. L. (2020a). Magnetohydrodynamic Casson Fluid Flow Past a Vertical Plate in the Presence of Thermal Conductivity and Chemical Absorption. International Journal of Science for Global Sustainability, 6(2), 82-91. https://doi.org/10.57233/ijsgs.v6i2.111

Omokhuale, E., & Jabaka, M. L. (2020b). Effect of Radiation on Heat and Mass Transfer Magnetohydrodynamic Casson fluid flow in a vertical channel. CaJoST, 2(2), 73-80.

Omokhuale, E., & Jabaka, M. L. (2022). Unsteady convective Couette flow with heat sink and radiation effects. FUDMA Journal of Sciences, 6(1), 266-277. https://doi.org/10.33003/fjs-2022-0601-873

Omokhuale, E., & Dange , M. S. (2025). Effects of heat generation and Soret on magnetohydrodynamic (MHD) Couette flow with radiation and mass absorption. International Journal of Science for Global Sustainability, 11(2), 86–96. https://doi.org/10.57233/ijsgs.v11i2.853

Reddy, B. P., Matao, P. M., & Sunzu, J. M. (2024). A finite difference study of radiative mixed convection MHD heat propagating Casson fluid past an accelerating porous plate including viscous dissipation and Joule heating effects. Heliyon, 10(7). https://doi.org/10.1016/j.heliyon.2024.e28591

Reddy, B. P., Shamshuddin, M. D., Salawu, S. O., & Matao, M. P. (2025). Cross-diffusion effects of viscous heating hydromagnetic Casson fluid flow in permeable vertical media with radiation and heat loss. Partial Differential Equations in Applied Mathematics, 14. https://doi.org/10.1016/j.padiff.2025.101225

Reddy, B. S., & Goud, B. S. (2026). Transportation of MHD Casson fluid with dissipation, radiation impact under Dufour effect over an exponentially stretching surface with activation energy: a numerical study. Modeling Earth Systems and

DOI: https://doi.org/10.57233/ijsgs.v12i2.1113 ISSNp: 2488-9229; ISSNe: 3027-1118

IJSGS FUGUSAU VOL . 12 (2) WEBSITE: https://fugus-ijsgs.com.ng

Environment, 12(1), 28. https://doi.org/10.1007/s40808-025-02677-5

Vinod, Y., Raghunatha, K. R., Nagappanavar, S. N., Nazarova, N., & Gupta, M. (2025). Boundary layer flow of a non-Newtonian fluid over an exponentially stretching sheet with the presence of a heat source/sink. Partial Differential Equations in Applied Mathematics, 13. https://doi.org/10.1016/j.padiff.2025.101111